

geometrical correlation length), and consequently a purely diffusive large-scale behaviour for the force. Therefore, we conclude that our results are certainly applicable to disordered packings such as cohesionless soils or sand piles. In contrast, for the particular case of non-random, textured packings, biased and long-range correlated q -series along the force transmission tree are likely to be encountered, thus altering the previous purely diffusive behaviour. □

Received 4 October 1999; accepted 15 June 2000.

- Ennis, B. J. in *Powders and Grains 97* (eds Behringer, R. P. & Jenkins, T. J.) 13–23 (A. A. Balkema, Rotterdam, 1997)
- Gray, J. M. & Hutter, K. Physik granularer Lawinen. *Phys. Bl.* **54**, 37–43 (1998).
- Terzaghi, K. *Theoretical Soil Mechanics* (Wiley, New York, 1943)
- Bouchaud, J. P., Cates, M. E. & Claudin, P. Stress distribution in granular media and nonlinear wave equation. *J. Phys. I (Fr.)* **5**, 639–656 (1995)
- Cates, M. E., Wittmer, J., Bouchaud, J. P. & Claudin, P. Development of stresses in cohesionless poured sand. *Phil. Trans. R. Soc. Lond. A* **356**, 2535–2560 (1998).
- Sokolovskii, V. V. *Statics of Granular Media* (Pergamon, New York, 1965).
- Timoshenko, S. & Goodier, J. N. *Theory of Elasticity* (McGraw Hill, New York, 1951)
- Landau, L. D. & Lifschitz, E. M. *Theory of Elasticity* (Pergamon, New York, 1980).
- Boussinesq, J. *Application des Potentiels à l'Étude de l'Équilibre et des Mouvements des Solides Élastiques* (Gauthier-Villars, Paris, 1885).
- Coppersmith, S. N., Liu, C. H., Majumdar, S., Narayan, O. & Witten, T. A. Model for force fluctuations in bead packs. *Phys. Rev. E* **53**, 4673–4685 (1996).
- Liu, C. H. *et al.* Force fluctuations in bead packs. *Science* **269**, 513–515 (1995).
- Miller, B., O'Hern, C. & Behringer, R. P. Stress fluctuations for continuous sheared granular packing. *Phys. Rev. Lett.* **77**, 3110–3113 (1996).
- Mueth, D. M., Jaeger, H. M. & Nagel, S. R. Force distribution in granular packing. *Phys. Rev. E* **57**, 3164–3169 (1998).
- Ngadi, A. & Rajchenbach, J. Intermittencies in the compression process of a model granular medium. *Phys. Rev. Lett.* **80**, 273–276 (1998).
- Radjai, F., Jean, M., Moreau, J. J. & Roux, S. Force distribution in dense two dimensional granular systems. *Phys. Rev. Lett.* **77**, 274–277 (1996).
- Peralta-Fabi, R., Malaga, C., Reichtman, R. in *Powders and Grains 97* (eds Behringer, R. P. & Jenkins, T. J.) 227–230 (A. A. Balkema, Rotterdam, 1997).
- Moukarzel, C. Isostatic phase transition and instability in stiff granular materials. *Phys. Rev. Lett.* **81**, 1634–1637 (1998).

Acknowledgements

We thank E. Bringuier for a critical reading of the manuscript.

Correspondence and requests for materials should be addressed to J.R. (e-mail: jer@ccr.jussieu.fr).

A colorimetric sensor array for odour visualization

Neal A. Rakow & Kenneth S. Suslick

Department of Chemistry, University of Illinois at Urbana-Champaign, 600 S. Mathews Avenue, Urbana, Illinois 61801, USA

Array-based vapour-sensing devices are used to detect and differentiate between chemically diverse analytes. These systems—based on cross-responsive sensor elements—aim to mimic the mammalian olfactory system^{1–3} by producing composite responses unique to each odorant. Previous work has concentrated on a variety of non-specific chemical interactions^{4–11} to detect non-coordinating organic vapours. But the most odiferous, toxic compounds often bind readily to metal ions. Here we report a simple optical chemical sensing method that utilizes the colour change induced in an array of metalloporphyrin dyes upon ligand binding while minimizing the need for extensive signal transduction hardware. The chemoselective response of a library of immobilized vapour-sensing metalloporphyrin dyes permits the visual identification of a wide range of ligating (alcohols, amines, ethers, phosphines, phosphites, thioethers and thiols) and even weakly ligating (arenes, halocarbons and ketones) vapours. Water

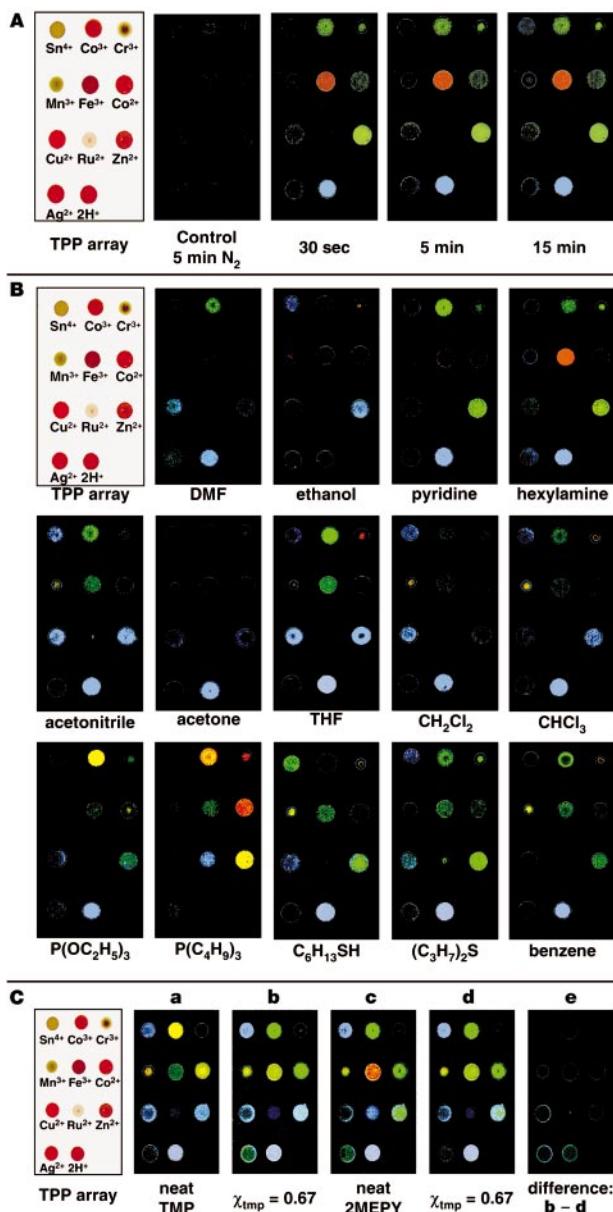


Figure 1 Colour change profiles of a metalloporphyrin sensor array. **A**, Colour change profiles of the metalloporphyrin sensor array as a function of exposure time to *n*-butylamine vapour. Metalloporphyrins were immobilized on reverse phase silica gel plates. Colour images were obtained with a flatbed scanner (HP Scanjet 3c) at 200 d.p.i. resolution. Subtraction of the initial scan from a scan after 5 min of N₂ exposure was used as a control, giving a black response, as shown. 9.3% *n*-butylamine in N₂ was then passed over the array and scans made after exposure for 30 s, 5 min and 15 min. The RGB mode images were subtracted (absolute value) using Adobe Photoshop software, with contrast enhancement by expanding the pixel range (a 32-value range was expanded to 256 each for the R, G and B values). **B**, Colour change profiles for a series of vapours; the degree of ligand softness (roughly their polarizability) increases from left to right, top to bottom. Each analyte was delivered to the array as a nitrogen stream saturated with the analyte vapour at 20 °C (to ensure complete saturation, vapour exposures of 15 min or greater were used). DMF, dimethylformamide; THF, tetrahydrofuran. **C**, Two component analysis; saturation responses to mixtures of 2-methylpyridine and trimethylphosphite. Vapour mixtures were obtained by mixing the analyte-saturated N₂ streams at variable flow ratios. A single plate was first exposed to pure trimethylphosphite vapour in N₂ (**a**), followed by increasing mole fractions of 2-methylpyridine up to pure 2-methylpyridine vapour (**c**), followed by decreasing mole fractions of 2-methylpyridine back to pure trimethylphosphite vapour. In both directions, scans were taken at the same mole fraction of trimethylphosphite (χ_{tmp}) and showed excellent reversibility; scans are shown at $\chi_{tmp} = 0.67$ (**b** and **d**), and their difference map is also shown (**e**).

vapour does not affect the performance of the device, which shows a good linear response to single analytes, and interpretable responses to analyte mixtures. Unique colour fingerprints can be obtained at analyte concentrations below 2 parts per million, and responses to below 100 parts per billion have been observed. We expect that this type of sensing array will be of practical importance for general-purpose vapour dosimeters and analyte-specific detectors (for insecticides, drugs or neurotoxins, for example).

Previous arrays have employed a variety of chemical interaction strategies, including the use of conductive polymers⁴, conductive polymer/carbon-black composites⁵, fluorescent dye/polymer systems^{6,7}, tin oxide sensors^{8,9} and polymer-coated surface acoustic wave devices^{10,11}. Although these systems have demonstrated success in chemical vapour detection and differentiation, their primary aim has been the detection of non-coordinating organic vapours. Many of the most toxic and certainly the most odiferous compounds, however, are excellent ligands for metal ions. Array detection of metal-binding species, such as amines, phosphines and thiols, has been much less explored. (We note that there are two obvious exceptions to the correlation between metal binding and olfactory sensitivity: NO and CO, both of which are produced endogenously as intercellular messenger molecules, and therefore should be olfactorily undetectable¹².) Although very little is known about the structures of the olfactory receptor proteins¹³, we speculate that many of the sensors are likely to contain metal ions at their active site.

Metalloporphyrins are a natural choice for the detection of metal-ligating vapours because of their open coordination sites for axial ligation, their large spectral shifts upon ligand binding, and their intense coloration. Metalloporphyrins have been previously employed for optical detection of gases such as oxygen^{13,14} and ammonia¹⁵, and for vapour detection as chemically interactive layers on quartz crystal microbalances^{16,17}. Here we have taken advantage of the large colour changes induced in metalloporphyrins upon ligand binding, and developed an easy colorimetric technique that minimizes the need for extensive signal transduction hardware. This represents, to our knowledge, the first example of a colorimetric array detector for vapour-phase ligands. Simply by taking the difference before and after exposure of scanned images of the array, we are able to obtain unique colour-change signatures for analytes; these signatures can be used for both qualitative recognition and quantitative analysis.

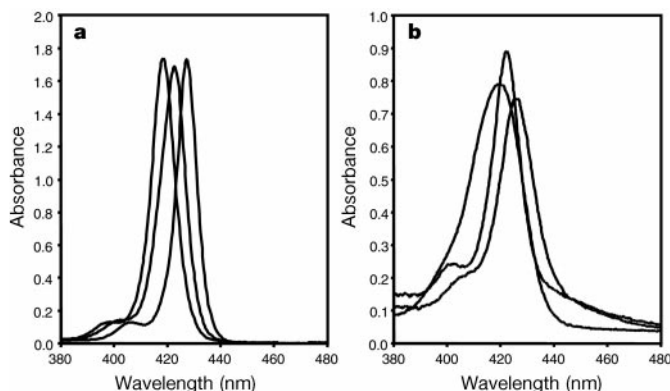


Figure 2 Comparison of Zn(TPP) spectral shifts upon exposure to ethanol and pyridine (py). **a**, In methylene chloride solution; **b**, on the reverse phase support. In both **a** and **b**, the bands correspond, from left to right, to Zn(TPP), Zn(TPP)(C₂H₅OH) and Zn(TPP)(py), respectively. Solution spectra (**a**) were collected using a Hitachi U-3300 spectrophotometer; Zn(TPP), C₂H₅OH and py concentrations were approximately 2 μM, 170 mM and 200 μM, respectively. Diffuse reflectance spectra (**b**) were obtained *in situ* with an integrating sphere attachment before exposure to analytes, after exposure to ethanol (5.8% in N₂), and after exposure to pyridine (2.1% in N₂) for 30 min.

Previous studies have elucidated the large spectral changes (and readily observable colour changes) that occur in solution during ligand binding to metalloporphyrins¹⁸. Solution studies have indicated that the magnitude of spectral shift correlates with the polarizability of the ligand¹⁹; hence, there exists an electronic basis for analyte distinction. Using metal centres that span a range of chemical ‘hardness’ and ligand-binding affinity, a wide range of volatile analytes should be differentiable. Because porphyrins show significant solvatochromic effects, even weakly interacting vapours (for example, arenes, halocarbons or ketones) show distinguishable colorimetric effects.

Solutions of various metalated tetraphenylporphyrins in either methylene chloride or chlorobenzene were spotted onto reverse phase silica thin-layer-chromatography plates to produce the sensor array shown in Fig. 1. The chosen metalloporphyrins have excellent chemical stability on the solid support, and most have well-studied solution ligation chemistry. A stainless-steel flow cell equipped with a quartz window held the plate in a fixed position on an inexpensive flatbed scanner, and permitted exposure of the plate to nitrogen carrying the vapour analyte of interest. Scanning after analyte exposure and subtracting new images from the original scan produces a colour change profile, such as that shown for *n*-butylamine in Fig. 1A. (Details of the image processing are given in Fig. 1 legend.) Virtually all porphyrins are saturated after 30 seconds of exposure, yielding a unique colour fingerprint.

In order to demonstrate the generality of this sensing technique, the vapours were chosen to represent a wide range of chemical functionalities. A comparison of colour changes at saturation for a wide range of analytes is shown in Fig. 1B. Each analyte is easily distinguished from the others, and there are family resemblances among chemically similar species (for example, pyridine and *n*-hexylamine). Analyte distinction originates both in the metal-specific ligation affinities and in their specific, unique colour changes upon ligation.

The metalloporphyrin array can also be used to quantify single analytes and to identify vapour mixtures. Because the images’ colour-channel data (that is, RGB values) vary monotonically with porphyrin concentration, we were able to quantify single porphyrin responses to different analytes. Colour-channel data were collected for individual spots and plotted as the quantity $(R_{\text{plt}} - R_{\text{spt}})/R_{\text{plt}}$, where R_{plt} was the red-channel value for the initial silica surface and R_{spt} the average value for the spot. A good linear response is observed until saturation for each porphyrin spot. For example, Zn(TPP), where TPP is 5,10,15,20-tetraphenylporphyrinate(-2), responded linearly to *n*-octylamine between 0 and 0.5 parts per million (p.p.m.). Other porphyrins showed linear response ranges that varied with ligand affinity. Quantifiable, reversible responses are observed even for analyte mixtures of strong ligands, such as pyridines and phosphites (Fig. 1C). Colour change patterns for the mixtures are distinct from either of the neat vapours. Good reversibility was demonstrated for this analyte pair as the vapour mixtures were cycled between the

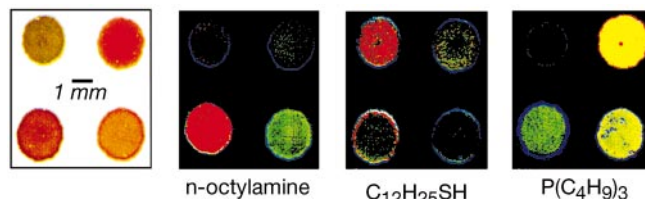


Figure 3 Colour fingerprints at low levels of analyte. The response of a minimized array of four metalloporphyrins (Sn(TPP)(Cl)₂, Co(TPP)(Cl), Zn(TPP) and Fe(TFP)(Cl)), clockwise from the upper left) is shown for *n*-octylamine, dodecanethiol and tri-*n*-butylphosphine at 1.8 p.p.m.

neat analyte extremes, as shown in Fig. 1C. Response curves of individual porphyrins with varying analyte composition provide a multicomponent analysis of mixtures. For example, for the trimethylphosphite/2-methylpyridine system, Co(TPP) responded linearly in this range to the mole fraction of trimethylphosphite, enabling quantification of an unknown blend of the two vapours.

In an effort to understand the origin of the colour changes upon vapour exposure, diffuse reflectance spectra were obtained for single porphyrin spots before and after exposure to analyte vapours. Porphyrin solutions were spotted in 50- μl aliquots onto a plate and allowed to dry under vacuum at 50 °C. Spectral shifts on the plate upon analyte exposure correlated well with those seen from solution ligation. For example, exposure of Zn(TPP) to ethanol and pyridine gave shifts very similar to those resulting from ligation in methylene chloride solutions (Fig. 2).

Reverse phase silica was initially chosen as a non-interacting dispersion medium for the metalloporphyrin array, as well as a suitable surface for diffuse reflectance spectral measurements. The hydrophobic nature of the support also greatly reduces interference from water vapour. For instance, a colour fingerprint generated from exposure of the array to *n*-hexylamine vapour (0.86% in N_2) was identical to that for *n*-hexylamine spiked heavily with water vapour (0.43% *n*-hexylamine plus 1.2% H_2O in N_2); see Supplementary Information for further details. The ability to easily detect species in the presence of a large water background represents a substantial advantage over mass-sensing techniques or methodologies that employ polar polymers as part of the sensor array.

Our array's responses come from selective and specific interactions between the analytes and the metalloporphyrin library. This is in marked contrast to the use of a single indicating fluorophore doped in a variety of matrices, where weak matrix-analyte interactions are required to provide selectivity^{6,7}. An advantage of utilizing chemoselective sensors in an array is that unique patterns can be identified at low vapour concentrations. As shown in Fig. 3, an array of four metalloporphyrins can very easily distinguish *n*-octylamine, dodecanethiol and tri-*n*-butylphosphine at 1.8 p.p.m. in N_2 . Colour changes of metalloporphyrins on reverse phase silica are slow at analyte exposures below 1 p.p.m. owing primarily to the time necessary to equilibrate the high surface area of the silica surface. As shown in Fig. 4, deposition of the metalloporphyrin library as films on Teflon provides an easy route to miniaturization and gives greatly improved response times. Deposition of spots of approximately 500- μm on a side present no difficulty; at this size a 20 \times 20 array can be interfaced to an inexpensive CCD (charge-coupled device) detector for device fabrication. Deposition by ink-jet

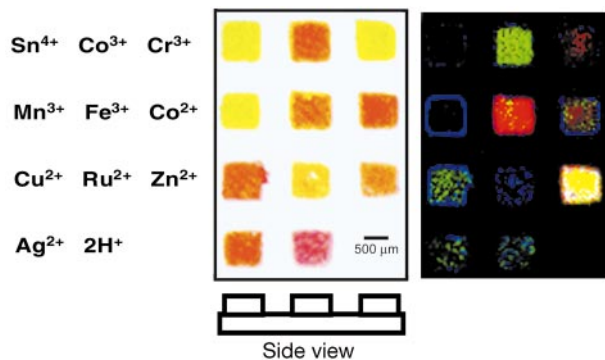


Figure 4 Miniaturized array. The metalloporphyrins were dissolved in a polymer film (dibutylphthalate in polystyrene) and deposited on Teflon; the miniaturization greatly reduces response times. On the left is the array before vapour exposure; on the right is the colour change profile after exposure to *n*-butylamine (1 min, 9.3% in N_2).

printing of these films should permit ready, and reproducible, production of chemoselective sensor arrays.

An important goal is the shape-selective distinction of analytes (for example, *n*-hexylamine versus cyclohexylamine). Functionalized metalloporphyrins that limit steric access to the metal ion^{20–22} are candidates for such differentiation. For instance, we have been able^{23,24} to control ligation of various inorganic ligands to dendrimer-metalloporphyrins and siloxyl-metalloporphyrins, and induce selectivities over a range of up to 10^7 . The initial results from a small library of siloxyl-metalloporphyrins reveal striking differences between analytes as similar as *n*-octylamine, cyclohexylamine and dipropylamine. Such shape-selective analyte discrimination should add a second tier of molecular recognition to the metal-based array.

The technique that we report here can differentiate between a wide range of species. Such 'smell-seeing' could have a number of different applications, including disposable general-purpose vapour dosimeters as well as analyte-specific detectors. The ability to target metal-binding species provides a complementary technique to currently developing methodologies for non-ligating organic vapours. We are at present working to optimize the array components, complete device fabrication, extend such analysis to liquids, and automate the pattern recognition. □

Methods

Porphyrin preparation

5,10,15,20-Tetraphenylporphyrin, H_2TPP , and its metal complexes were prepared using published methods^{25–28}, and fully characterized by fast-atom-bombardment mass spectrometry, elemental analysis, and ultraviolet-visible and NMR spectroscopies. 5,10,15,20-Tetrakis(pentafluorophenyl)-porphyrinatoiron(III) chloride, Fe(TFPF)(Cl), (purchased from Aldrich and used as-received) was added to the porphyrin array because it shows higher ligand-binding constants.

Porphyrin immobilization

The porphyrin array was spotted onto C2 reverse phase silica gel thin-layer-chromatography plates (Whatman KC2, 200 μm thickness, 350 $\text{m}^2 \text{g}^{-1}$ surface area). Porphyrins were spotted from solutions (of a few mM) in chlorobenzene or methylene chloride using a 1- μl microcapillary tube or microlitre syringe. After spotting, sensor plates were dried under vacuum at 50 °C for 1 h before use.

Vapour exposure

Gas streams containing the vapour of interest were generated by flowing nitrogen at 0.5 min^{-1} through the neat liquid analyte in a water-jacketed, glass fritted bubbler. All liquid analytes were obtained from Aldrich or Fisher Scientific, and used as-received. Vapour pressures were controlled by regulating the bubbler temperature²⁹. Low p.p.m. levels of *n*-octylamine and tri-*n*-butylphosphine were generated from temperature-regulated analyte/dodecane solutions with the assumption of solution ideality.

Received 25 November 1999; accepted 25 May 2000.

- Dryer, L. & Berghard, A. Odorant receptors: a plethora of G-protein-coupled receptors. *Trends Pharmacol. Sci.* **20**, 413–417 (1999).
- Lancet, D. & Ben-Arie, N. Olfactory receptors. *Curr. Biol.* **3**, 668–674 (1993).
- Axel, R. The molecular logic of smell. *Sci. Am.* **273**, 154–159 (1995).
- Freund, M. S. & Lewis, N. S. A chemically diverse conducting polymer-based "electronic nose". *Proc. Natl Acad. Sci. USA* **92**, 2652–2656 (1995).
- Loneragan, M. C. *et al.* Array-based vapor sensing using chemically sensitive, carbon black-polymer resistors. *Chem. Mater.* **8**, 2298–2312 (1996).
- Walt, D. R. Fiber optic imaging sensors. *Acc. Chem. Res.* **31**, 267–278 (1998).
- Dickinson, T. A., White, J., Kauer, J. S. & Walt, D. R. A chemical-detecting system based on a cross-reactive optical sensor array. *Nature* **382**, 697–700 (1996).
- Heilig, A. *et al.* Gas identification by modulating temperatures of SnO_2 -based thick film resistors. *Sens. Actuators B* **43**, 45–51 (1997).
- Gardner, J. W., Shurmer, H. V. & Tan, T. T. Application of an electronic nose to the discrimination of coffees. *Sens. Actuators B* **6**, 71–75 (1992).
- Crooks, R. M. & Ricco, A. J. New organic materials suitable for use in chemical sensor arrays. *Acc. Chem. Res.* **31**, 219–227 (1998).
- Grate, J. W. & Abraham, M. H. Solubility interactions and the design of chemically selective sorbent coatings for chemical sensors and arrays. *Sens. Actuators B* **3**, 85–111 (1991).
- Gelperin, A., Flores, J. & Raccuia-Behling, F. Nitric oxide and carbon monoxide modulate oscillations of olfactory interneurons in a terrestrial mollusk. *J. Neurophysiol.* **83**, 116–127 (2000).
- Baron, A. E., Danielson, J. D. S., Gouterman, M., Wan, J. R. & Callis, J. B. Submillisecond response times of oxygen-quenched luminescent coatings. *Rev. Sci. Instrum.* **64**, 3394–3402 (1993).
- Lee, W. *et al.* Halogenated platinum porphyrins as sensing materials for luminescence-based oxygen sensors. *J. Mater. Chem.* **3**, 1031–1035 (1993).
- Vaughan, A. A., Baron, M. G. & Narayanaswamy, R. Optical ammonia sensing films based on an immobilized metalloporphyrin. *Anal. Commun.* **33**, 393–396 (1996).

16. Brunink, J. A. J. *et al.* The application of metalloporphyrins as coating material for quartz microbalance-based chemical sensors. *Anal. Chim. Acta* **325**, 53–64 (1996).
17. Di Natale, C. *et al.* The exploitation of metalloporphyrins as chemically interactive material in chemical sensors. *Mater. Sci. Eng. C* **5**, 209–215 (1998).
18. Blauer, G. & Sund, H. (eds) *Optical Properties and Structure of Tetrapyrroles* (de Gruyter, Berlin, 1985).
19. Nappa, M. & Valentine, J. S. The influence of axial ligands on metalloporphyrin visible absorption spectra. Complexes of tetraphenylporphinatozinc. *J. Am. Chem. Soc.* **100**, 5075–5080 (1978).
20. Suslick, K. S. & Van Deussen-Jeffries, S. in *Comprehensive Supramolecular Chemistry* (ed. Lehn, J. M.) 141–170 (Elsevier, Oxford, 1996).
21. Bhyrappa, P., Young, J. K., Moore, J. S. & Suslick, K. S. Dendrimer porphyrins: synthesis and catalysis. *J. Am. Chem. Soc.* **118**, 5708–5711 (1996).
22. Chou, J.-H., Nalwa, H. S., Kosal, M. E., Rakow, N. A. & Suslick, K. S. in *The Porphyrin Handbook* (eds Kadish, K., Smith, K. & Guillard, R.) 43–132 (Academic, New York, 2000).
23. Bhyrappa, P., Vijayanthimala, G. & Suslick, K. S. Shape-selective ligation to dendrimer-metallporphyrins. *J. Am. Chem. Soc.* **121**, 262–263 (1999).
24. Sen, A. & Suslick, K. S. Shape selective discrimination of small organic molecules. *J. Am. Chem. Soc.* (in the press).
25. Adler, A. D. *et al.* A simplified synthesis for meso-tetraphenylporphyrin. *J. Org. Chem.* **32**, 476 (1967).
26. Adler, A. D., Longo, F. R., Kampas, F. & Kim, J. On the preparation of metalloporphyrins. *J. Inorg. Nucl. Chem.* **32**, 2443–2445 (1970).
27. Barley, M., Becker, J. Y., Domazetis, G., Dolphin, D. & James, B. R. Synthesis and redox chemistry of octaethylporphyrin complexes of ruthenium(II) and ruthenium(III). *Can. J. Chem.* **61**, 2389–2396 (1983).
28. Datta-Gupta, N. & Bardos, T. J. Synthetic porphyrins II: preparation and spectra of some metal chelates of para-substituted-meso-tetraphenylporphyrins. *J. Pharm. Sci.* **57**, 300–304 (1968).
29. Yaws, C. L. *Handbook of Vapor Pressure* (Gulf, Houston, 1994).

Supplementary Information is available on Nature's World-Wide Web site (<http://www.nature.com>) or as paper copy from the London editorial office of Nature.

Acknowledgements

This work was supported by the US NIH and in part by the US DOD and DOE.

Correspondence and requests for materials should be addressed to K.S.S. (e-mail: ksuslick@uiuc.edu).

.....
Timing of the Last Glacial Maximum from observed sea-level minima

Yusuke Yokoyama*†, Kurt Lambeck*, Patrick De Deckker‡, Paul Johnston* & L. Keith Fifield§

* *Research School of Earth Sciences*, ‡ *Department of Geology*, § *Department of Nuclear Physics, Research School of Physical Sciences and Engineering, The Australian National University, Canberra, ACT 0200, Australia*

.....
During the Last Glacial Maximum, ice sheets covered large areas in northern latitudes and global temperatures were significantly lower than today. But few direct estimates exist of the volume of the ice sheets, or the timing and rates of change during their advance and retreat^{1,2}. Here we analyse four distinct sediment facies in the shallow, tectonically stable Bonaparte Gulf, Australia—each of which is characteristic of a distinct range in sea level—to estimate the maximum volume of land-based ice during the last glaciation and the timing of the initial melting phase. We use faunal assemblages and preservation status of the sediments to distinguish open marine, shallow marine, marginal marine and brackish conditions, and estimate the timing and the mass of the ice sheets using radiocarbon dating and glacio-hydroisostatic modelling. Our results indicate that from at least 22,000 to 19,000 (calendar) years before present, land-based ice volume was at its maximum, exceeding today's grounded ice sheets by $52.5 \times 10^6 \text{ km}^3$. A rapid decrease in ice volume by about 10% within a few hundred years terminated the Last Glacial Maximum at $19,000 \pm 250$ years.

† Present address: Space Sciences Laboratory, University of California, Berkeley, California, USA, and Lawrence Livermore National Laboratory, 7000 East Avenue, PO Box 808, L-202 Livermore, California 94550, USA.

The broad and shallow continental margin of northern Australia includes several local bathymetric depressions, the largest of which is the Bonaparte Gulf. During times of sea-level lowstands much of the shelf was exposed, and the sediments deposited in the depressions were protected from wave action by the outer shelf edge. A total of 23 gravity cores, 10 vibrocores and 3 grab samples were collected from present-day water depths of 34 to 147 m along transects across the shelf margin and the Bonaparte depression (Fig. 1a). All cores were sedimentologically examined and a number were selected for micropalaeontological analysis and radiocarbon dating. Depending on faunal assemblages and preservation status (Fig. 1b, see also Methods section below) four distinct bio-sedimentary facies have been recognized: open marine, shallow marine, marginal marine, and brackish water, denoted by OM, SM, MM and BR, respectively, in Fig. 1b. We obtained 41 radiocarbon dates of foraminifera and bivalve molluscs using accelerator mass spectrometry (AMS) techniques and dated some of the larger bivalves using conventional liquid scintillation counting methods. All AMS-dated samples were severely etched (about 40% to 50%) to discard outer shell material that may have been contaminated by secondary carbonate precipitation. Figure 1b summarizes the results for 7 of the cores from water depths between 128 and 95 m. All carbonate ages have been corrected for reservoir effect (400 years; refs 3, 4) and calibrated to a calendar timescale^{5,6}. The cores indicate excellent preservation of faunal specimens, many without evidence for reworking, and the ¹⁴C dates indicate only rare instances of age inversions.

Last Glacial Maximum (LGM) sea-level indicators are preserved in a number of the cores. To reconstruct a sea-level curve based on micropalaeontological evidence, it is necessary to consider the palaeoenvironmental conditions as a sequence of events assuming that little or no break in sedimentation, and no erosion, has occurred. (If a hiatus does occur it results in missing bio-facies and in reworking of the faunas; and this is not observed.) Thus, through identification of a transition from shallow marginal marine to brackish conditions and then back to shallow marginal marine conditions, the timing of the brackish conditions records the interval of lowest sea level. Once this depth is identified in a single core, other cores with depths either side of the identified low sea-level stand are examined to substantiate the reconstruction. This has been done using core GC5 as the master core because it has the best preserved and dated record for brackish water conditions. No truly lacustrine phase has been recognised in any of the cores, indicating that throughout the LGM the Bonaparte depression remained in open contact with the Timor Sea⁷.

The transition from marginal marine to brackish facies occurs in core GC5 at 21,280 calendar years before present (cal. yr BP) at a depth of 340 cm below the sea floor (Fig. 1b). Sediments below this depth contain marine ostracods and planktonic foraminifers, whereas above this boundary dwarf specimens of the benthic foraminifer *Ammonia beccarii* occur along with other shallow to brackish water indicators such as the benthic foraminifer *Elphidium* spp. and the euryhaline ostracod *Cyprideis australiensis*^{8,9}. Marginal marine and brackish-water conditions existed for about 3,000 years, in agreement with results from cores GC4 and GC6 (Fig. 1b) as well as GB1. Sea level at GC5 was, therefore, a few metres below -121 m (Fig. 2a) in this time interval. Deeper cores, both within the depression (GC1, GC2 and GC3) and outside it, do not indicate any brackish facies and place a lower limit of -125 m on the position of relative sea-level at these locations. The microfossil assemblages of cores GC10 and GC11, at -103 and -101 m respectively, are indicative of a marginal beach or coastal lagoon environment between 17,650 and 17,450 cal. yr BP. In core GC7, undamaged littoral-dwelling bivalves occur at -107 m with an age of 17,610 cal. yr BP (Fig. 1b). Figure 2a illustrates the results for all samples free from post-depositional disturbance. They indicate that between 22,000 and 19,000 cal. yr BP a rapid rise of 10–15 m occurred.